Soft Pneumatic Actuator from 3D-Printed TPU: Fabrication and Grasping Force Characterization

Ken Kanate Wichiramala
International School of Engineering
Chulalongkorn University
Bangkok, Thailand

Siwakorn Opasjirawiroj
International School of Engineering
Chulalongkorn University
Bangkok, Thailand

Nattawat Chongpita
International School of Engineering
Chulalongkorn University
Bangkok, Thailand

Ronnapee Chaichaowarat *
International School of Engineering
Chulalongkorn University
Bangkok, Thailand
ronnapee.c@chula.ac.th

***Abstract*—Soft pneumatic actuators providing infinite passive degrees of freedom are widely applied for safe physical human–robot interaction and fulfilling the limitation of conventional rigid structures. This paper presents a design of the soft actuator with pneumatic chamber enabling the control of bending and contact force. The actuator is solely fabricated from the thermoplastic polyurethane (TPU 95A) by using the fused deposition modeling (FDM) 3D printing. Several printing setups were performed for trial and error to prevent the air leak. The experimental setup was prepared for measuring the contact force in both vertical and horizontal directions. The grasping force varying against the input pressure ranged from 0 to 58 psi was studied at three contacting points along the longitudinal axis of the actuator with three different bending conditions. The stiffness of the actuator is related to the input pressure by considering the increase of total contacting force at different bending deformations. The results of this study can be applied to the stiffness control of soft pneumatic actuators.**

Keywords—Pneumatic actuator, soft gripper, 3D printing, stiffness modulation

I. Introduction

In today's world of robotics, safety is a primary concern of robots interacting with human counterparts and unknown environment [1]. For example, physical coupling always exists between the user and the lower-extremity exoskeletons [2] [3] or the gait rehabilitation robots [4]. Appropriate modulation of the mechanical impedance to tradeoff between safety and performance can be achieved by using feedback control [5] [6] and by adjusting the intrinsic properties of actuators such as equilibrium position, stiffness [7] [8], and damping [9]. The parallel elastic actuation concepts for reducing the power required from the human [10] or the motor peak torque [11] allow downsizing the actuator and gear ratio.

Rigid robotic manipulators have widely been used for manufacturing processes in structured environments. The advances in physical human–robot interaction allow the safe usage of manipulators in close proximity with humans in shared environments. There is a growing demand for soft robotic actuators that are capable of providing a more compliant and dynamic range of motion than traditional rigid robots. Soft actuators are commonly fabricated through mold casting of elastomeric materials, typically silicone rubber. The soft actuators were fabricated from silicone with a chamber-based structure by using a mold [12]. The tendon-driven origami pump was used instead of an external air compressor. However, the mapping between the height of the pump against the deformation of the actuator is nonlinear. Also, significant hysteresis was observed from the origami pump with limited amount of working airflow. The manufacturing process involves manual processing after the material is cured, which increases cost, time, and labor. The molding process also restricts design complexity and hinders design changes [13]. The fused deposition modeling (FDM) technology has enabled the development of a variety of soft actuators. The automated 3D printing technology is more cost-effective and allows complex designs of pneumatic actuators [14] for achieving higher output force and more complex movements.

The thermoplastic polyurethane (TPU) providing the performance characteristics of rubber with high elasticity and abrasion resistance was used for underwater manipulation [15]. The TPU materials of different Shore hardness ranged from 70A to 98A were compared. The flexible thermoplastic using additive manufacturing tool allows increasing the force applied with much less strain than silicone rubbers without requiring additional reinforcement. The tendon driven soft robotic gripper was fabricated by FDM printing of TPU structures with integrated strain sensing elements. The effect of TPU Shore hardness on the soft piezoresistive sensor properties was also studied [16]. The soft pneumatic actuator was developed for the universal robot gripper [17]. The radius of curvature and the bending performance were characterized. The soft pneumatic chamber with bioinspired fin-ray structure was presented for conformal grasping [18]. The bending motion against the input pressure (from 0-300 kPa) was compared between experiment and finite element simulation.

In this paper, a design of the soft actuator with pneumatic chamber enabling the control of bending and contact force is presented. The actuator was completely fabricated from the thermoplastic polyurethane (TPU 95A) by using the fused deposition modeling (FDM) 3D printing. Several printing setups were performed for trial and error to prevent the air leak. The grasping force varying against the input pressure ranged from 0 to 58 psi was studied at three contacting points along the longitudinal axis of the actuator with three different bending. In addition to the contact force, the stiffness of the pneumatic actuator was also estimated by considering the increase of force at different bending deformations.

The first, second, and third authors contributed equally to this work.

This paper is organized as follows: Section II explains the design and fabrication technique of the pneumatic gripper. Section III describes the hardware setup for grasping force characterization. Section IV discusses the experimental results and Section V summarizes the key findings.

II. Design and Fabrication

A. The Soft Pneumatic Actuator

In this study, the actuator (see Fig. 1) was designed with 16 identical air chambers embedded inside the actuator body and one large air chamber inside the actuator tip. These air chambers are connected by seven air channels located at the bottom layer. This arrangement ensures that the pressure from the air channels is uniformly distributed among each air chamber. When the actuator is inflated, the applied pressure causes the air chambers to expand. However, due to the presence of a solid wall at the bottom layer, the actuator bends downward.

The Raise3D E2 printer was used for printing the Polymaker PolyFlex™ TPU95 flexible filament. To achieve the design goal of an airtight actuator, the flow rate of the filament was raised to 130% of the normal flow rate, and a hot extruder temperature of 230 °C was used to increase layer adhesion. The important printing parameters are summarized in Table I. A captured screen from the ideaMaker slicer is shown in Fig. 2. We discovered that increasing the layer height did not reduce the occurrence of leakage, and it also resulted in a poor surface finish for the printed object. Therefore, the layer height of 0.3 mm was chosen as it accelerated the printing process and reduced the occurrence of leakage at the layer interface. To further mitigate leakage, four shells were implemented as one of the printing parameters. It was found that using a larger nozzle size did not make the actuator more airtight. Therefore, the nozzle size of 0.4 mm was selected because it provides high resolution for the design and allows for the fabrication of thinner walls without leakage.

TABLE I. Printing Parameters of Soft Pneumatic Actuator

Parameter	*Value*	*Unit*
Layer height	0.3	mm
Shell	4	layers
Extrusion width	0.4	mm
Infill density	20	%
Infill operlap	30	%
Heated bed temperature	60	°C
Extruder temperature	230	°C
Filament flowrate	130	%

The actuator has overall dimensions of 113 mm in length, 36 mm in width, and an air chamber height of 22.5 mm. The reference research paper suggested that the wall thickness of the actuator should be three times the size of nozzle size. Therefore, our wall thickness is 1.2 mm. The thickness of the bottom layer was set to 2.75 mm to assist the bending characteristic of the actuator.

B. The Actuator Holder

To provide a connection to the air supply, a pneumatic coupling was installed on the actuator. This was achieved by using 3D printed PLA brackets to engage with the flap on the actuator body. Screw mounting was used to provide tension and prevent leakage.

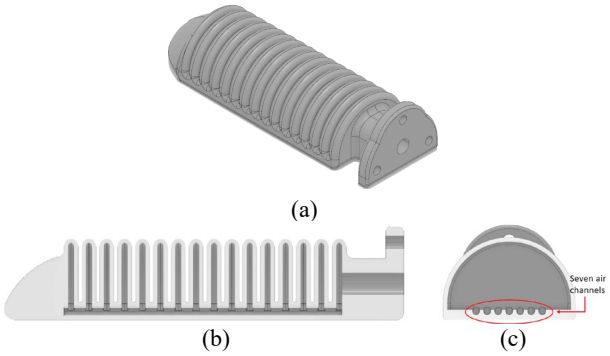

Fig. 1. Overview of the design: (a) Soft pneumatic actuator. (b) Crossed-section view of the soft actuator. (c) Seven air channels of the soft actuator.

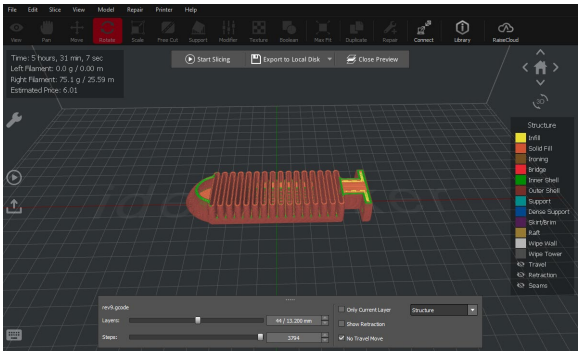

Fig. 2. The printing layer cross section of the soft pneumatic actuator captured from the ideaMaker slicer.

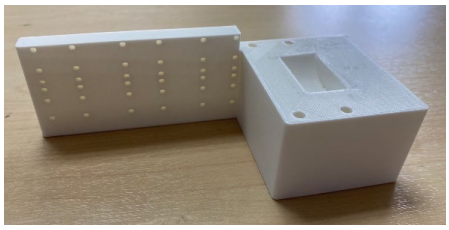

Fig. 3. The soft actuator holder with multiple mounting positions for the force sensor.

To understand the behavior of the soft pneumatic actuator after pressure is applied, it was necessary to design a soft actuator holder. This holder was designed to facilitate the understanding of the actuator's behavior through experimentation. The soft actuator holder, which was printed from PLA as shown in Fig. 3, had a semicircular hole for connecting to the soft actuator and available slots, each with four holes, for connecting to the Tec Gihan's USL06-H5 three-axis force sensor.

For this experiment, there are five testing positions. The first testing position was the upper-tip where the position of the M3 screw, inserted into the middle of the force sensor, was located 85 mm away from the origin, as shown in Fig. 4(a). The second testing position was the upper-middle where the position of the M3 screw was located 48 mm away from the origin, as shown in Fig. 4(b). The third testing position was the upper-base where the position of the M3 screw was located 11 mm away from the origin, as shown in Fig. 4(c). These three testing positions shared the same vertical axis, where the middle of the M3 screw was located 1.5 mm away from the lowest part of the soft actuator. This was to ensure that the highest point of the M3 screw contacted the lowest part of the soft actuator, thereby keeping the actuator parallel to the ground.

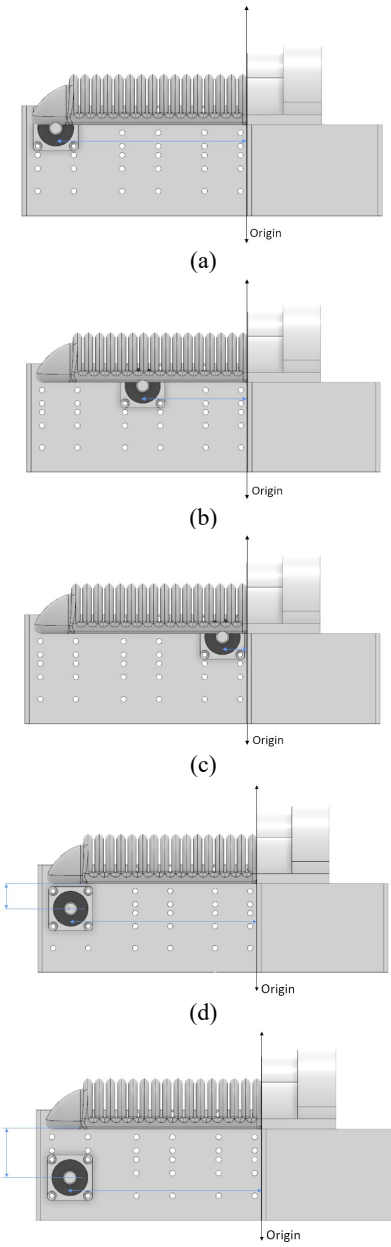

Fig. 4. Five testing positions: (a) Upper-tip, (b) Upper-middle, (c) Upper-base, (d) Middle-tip, and (e) Bottom-tip.

The fourth testing position was the middle-tip, where it shares the same horizontal alignment as the first testing position and has the position of the M3 screw located 11.5 mm below the lowest part of the soft actuator, as shown in Fig. 4(d). The fifth testing position was the bottom-tip, where it shares the same horizontal alignment as the first testing position and has the position of the M3 screw located 21.5 mm below the lowest part of the soft actuator, as shown in Fig. 4(e).

III. Experimental Setup

A. Hardware Configuration

Diagram in Fig. 5 shows the hardware setup in our experiment. The air supply source for the soft pneumatic actuator was the PUMA FORCE 35 air compressor, which had a power rating of 1450W and a capacity of 35L. When the soft actuator received the air supply, it underwent bending and interacted with the sensor screw, establishing an

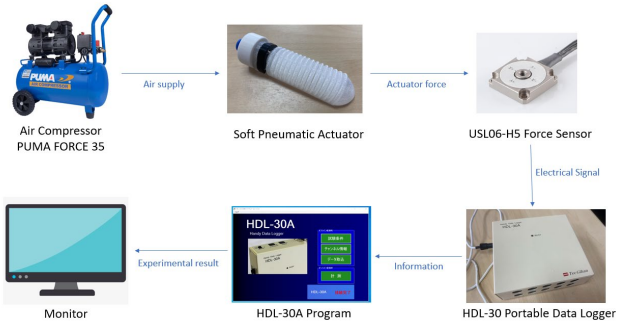

Fig. 5. Overview of the hardware system.

Fig. 6. Captured screen showing force data from the HDL-30A program.

action-reaction force relationship. The actuator force, which acted as the action force, was measured when it reached equilibrium with the reaction force exerted by the screw.

The force measured by the force sensor was transmitted to the HDL-30 Portable Data Logger as an electrical signal. The HDL-30A Program is served the purpose of receiving information from the data logger and converting it into graphical results displayed on the monitor, as shown in Fig. 6. In this case, the actuator force was represented as the graphical outcome of the experiment. The actuator force consisted of both the vertical force exerted by the actuator to push the screw downward and the horizontal force attempting to pull the sensor screw towards the origin.

B. Experimental Method

Since there were five testing positions as shown in Fig. 4. We tested positions 4(a), 4(b), and 4(c), which shared the same vertical alignment, to find the variation of actuator force at the upper segment positions when the horizontal distance was changed. We also tested positions 4(d) and 4(e) and used these testing results with the result from position 4(a) because these three positions shared the same horizontal alignment. This was to find the variation of actuator deformation at the tip segment positions when the vertical distance was changed.

The soft actuator was actuated as shown in Fig. 7 and the experimental procedure consists of the following steps:

- Initial Reset: The HDL-30A program, as shown in Fig. 6, was initiated by clicking the “zero” button to reset all graphs to the initial state, where the forces exerted on all axes were set to zero. The gravitational force of the soft actuator was neglected after clicking the “zero” button.
- Pressure Setup: The air compressor regulator knob was adjusted to achieve a pressure reading of 1 bar (14.5

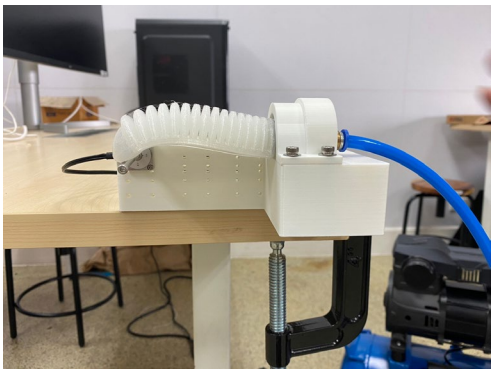

Fig. 7. The soft actuator after being actuated.

psi) on the pressure gauge. This pressure was maintained for a duration of 60 seconds. Subsequently, the program displayed the actuator force information.

- Repetition: The experimental procedure was repeated four additional times, ensuring a total of five repetitions at the 1 bar pressure setting. Each repetition involved resetting the system to its initial state, followed by the maintenance of the pressure for 60 seconds. This approach ensured the collection of reliable and consistent data across multiple trials.
- Pressure Variation: The experiment was then repeated for pressures of 2 bar (29.0 psi), 3 bar (43.5 psi), and 4 bar (58.0 psi), respectively. Similarly, the program displayed the actuator force information for each trial. However, in the case of the 4-bar pressure, the pressure was maintained for 20 seconds to prevent the pressure tank from recharging. This precaution aimed to avoid any potential influence on the reaction force of the sensor, thus ensuring accurate measurements.
- Testing on Other Sensor Positions: The entire experimental procedure was systematically repeated for each of the other testing positions, ensuring comprehensive coverage across all positions. The same set of steps, including the initial reset, pressure setup, repetition, and pressure variation was carried out for each position.

IV. Experimental Results

A. *Behavior of the Soft Pneumatic Actuator*

The shape of the soft pneumatic actuator is changed according to the input pressure for the following testing positions: the upper-tip position (see Fig. 8), the upper-middle position (see Fig. 9), the upper-base position (see Fig. 10), the middle-tip position (see Fig. 11), and the middle-bottom position (see Fig. 12).

In Fig. 10, the actuator force at the upper-base position at the 4 bar pressure was not included in the experimental results because the tip of the soft actuator contacted the actuator holder. This scenario affected the action-reaction force relationship between the soft actuator and the sensor screw, resulting in the deviation of the actuator force.

In Fig. 12, the actuator force at the bottom-tip position under 4 bar pressure was not included in the experimental results because the actuator can be tested for a very short time. After that the actuator was slipped off from the sensor screw which make the experiment unable to record the reaction force.

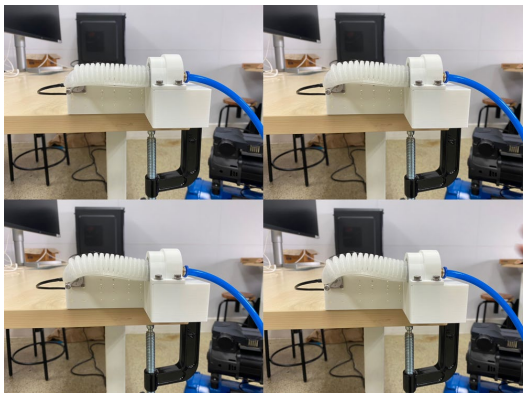

Fig. 8. The behavior of the actuator at the upper-tip position under different pressure conditions—1 bar, 2 bar, 3 bar, and 4 bar, respectively.

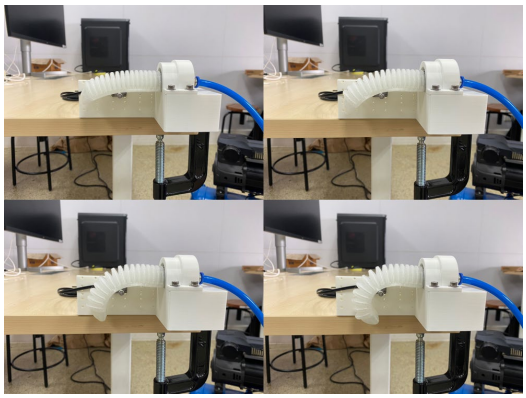

Fig. 9. The behavior of the actuator at the upper-middle position under different pressure conditions—1 bar, 2 bar, 3 bar, and 4 bar, respectively.

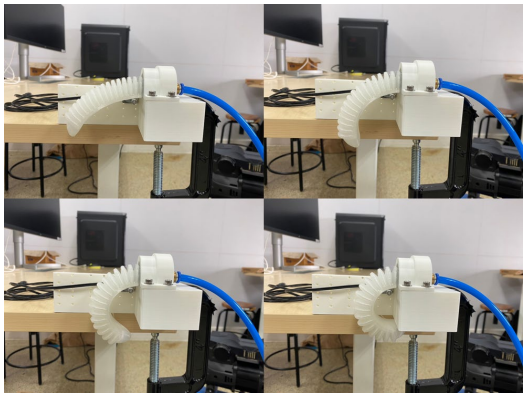

Fig. 10. The behavior of the actuator at the upper-base position under different pressure conditions—1 bar, 2 bar, 3 bar, and 4 bar, respectively.

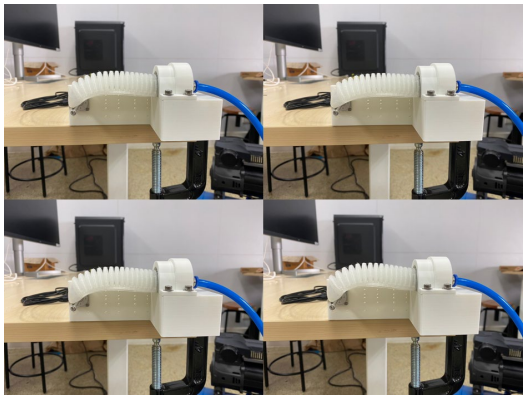

Fig. 11. The behavior of the actuator at the middle-tip position under different pressure conditions—1 bar, 2 bar, 3 bar, and 4 bar, respectively.

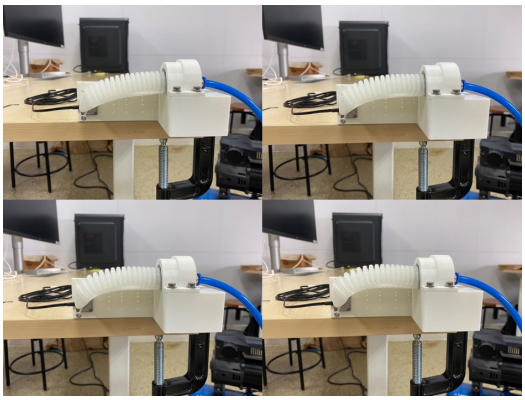

Fig. 12. The behavior of the actuator at the bottom-tip position under different pressure conditions—1 bar, 2 bar, 3 bar, and 4 bar, respectively.

B. Contact Force and Input Pressure Relationship at the Upper Segment

The contact force (vertical, horizontal, and total) varying against the input pressure at the three upper segment positions are shown in Fig. 13, respectively. The scatter plots in Fig. 14 show the relationship between the forces and the horizontal distance of the sensor away from the base, at the pressures of 1 bar, 2 bar, 3 bar, and 4 bar. The experiments were repeated for five trials.

At the upper-tip position, the vertical, horizontal, and total forces increase proportionally with the input pressure. The curvature deformation is observed (see Fig. 8), as the actuator tries to push the force sensor toward the base, which results in the increase of horizontal force.

At the upper-middle position, the effect of the curvature deformation is more dominant (see Fig. 9). The horizontal force increases with the input pressure while the positive relationship cannot be guaranteed for the vertical force.

At the upper-base position, the actuator force mostly occurs in the vertical direction. Because the force sensor position is so close to the base (see Fig. 10) that the actuator cannot bend enough to create the horizontal force.

C. Contact Force and Input Pressure Relationship at the Tip Segment

The contact force (vertical, horizontal, and total) varying against the input pressure at the other two tip segment positions are shown in Fig. 15, respectively. The scatter plot in Fig. 16 shows the relationship between the vertical force and the vertical distance of the sensor away from the top position, at the pressures of 1 bar, 2 bar, 3 bar, and 4 bar. The experiments were repeated for five trials. The results of the zero vertical distance are completely obtained from the upper-tip position.

At the middle-tip position, the effect of curvature deformation is observed (see Fig. 11). Although the positive relationship between the pressure and the vertical force can be observed (in Fig. 16), the differences in magnitude are very small. The stiffness of actuator (as a result of the input pressure) can be approximated from the slope of the linear trendline connecting the vertical force at different vertical distances between the upper-tip and the middle-tip positions.

At the bottom-tip position, the effect of curvature deformation is so significant (see Fig. 12) that the vertical force cannot be controlled by the input pressure. Initially, the force sensor is located far from the actuator (with zero input

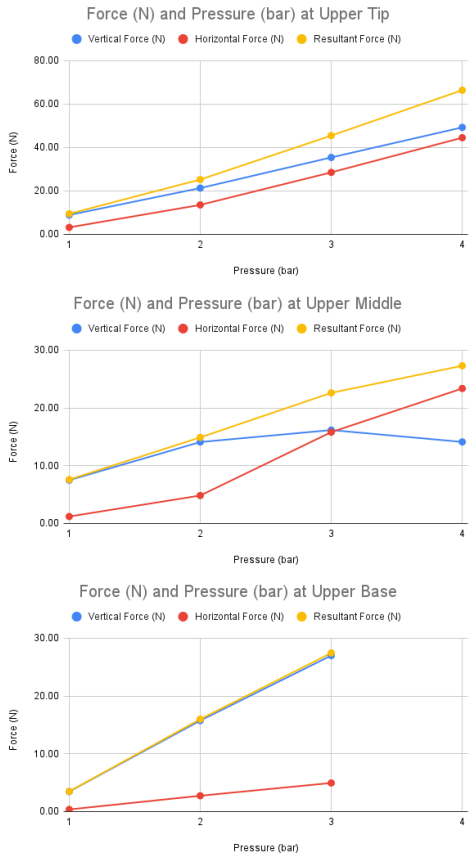

Fig. 13. The relationships between forces (vertical, horizontal, and total) and input pressure at the three upper segment positions.

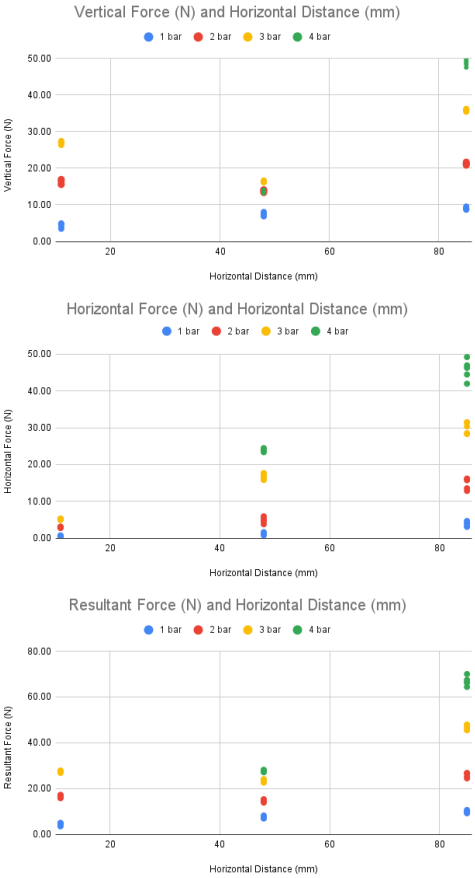

Fig. 14. The relationships between forces (vertical, horizontal, and total) and the horizontal distance from the base at the three upper segment positions.

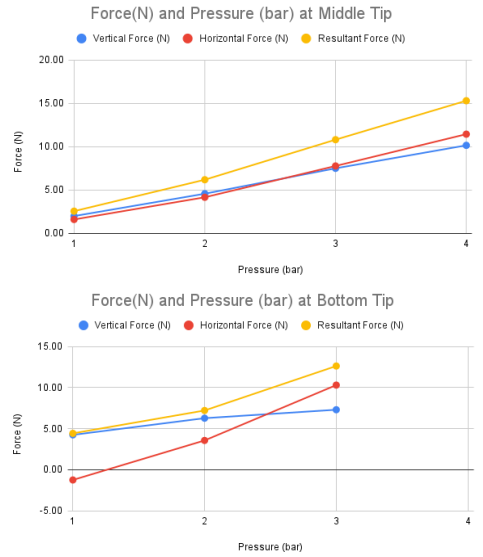

Fig. 15. The relationships between forces (vertical, horizontal, and total) and input pressure at the other two tip segment positions.

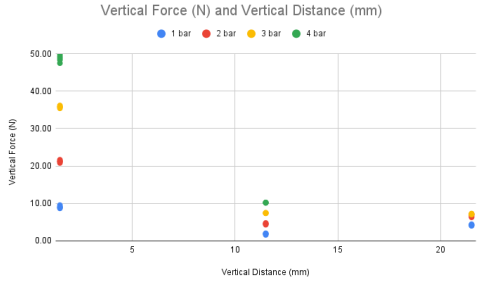

Fig. 16. The relationships between forces (vertical, horizontal, and total) and the vertical distance from the lowest position at the three tip segment positions.

pressure). The applied pressure is enough to bend the actuator to touch the force sensor but cannot provide significant magnitude of contact force.

V. Conclusion

By using the design constraints and printing parameters as presented, the functional soft pneumatic actuator was fabricated. The bending of the actuator is controlled through the pneumatic pressure without the air leak, which allows us to conduct experiments for characterizing the actuator. There are three sets of experimental results. First is the relationship between the input pressure and the actuator force, which is observed at different locations and bending conditions. At any certain position, the resultant force tends to increase linearly with the pressure although the vertical and the horizontal forces are sometimes converted between each other at extreme bending. Second is the effect of the horizontal distance (measured from the actuator base) on the actuator force, which is observed at different pressures. The resultant force tends to increase while measured at positions far from the base. Lastly, the stiffness of the pneumatic actuator is observed through the actuator force varying against the vertical distance (deviated from the horizontal baseline). At the tip position, the stiffness of the actuator increases with the pressure when the bending deformation is less than 12 mm. The results of this study can be used as a reference for controlling the stiffness of soft pneumatic actuators, which can further be applied in several robotic systems e.g., intelligent grippers [19] and legged robots [20].

Acknowledgement

This research project is partly supported by Tronormos Co., Ltd., Bangkok, Thailand and Tirawat Air Compressors Co., Ltd., Bangkok, Thailand.

References

[1] R. Chaichaowarat, S. Nishimura, T. Nozaki, and H. I. Krebs, "Work in the time of Covid-19: actuators and sensors for rehabilitation robotics," *IEEJ J. Ind. Appl.*, vol. 11, no. 2, pp. 1–10, 2021.

[2] R. Chaichaowarat, S. Prakthong, and S. Thitipankul, "Transformable wheelchair–exoskeleton hybrid robot for assisting human locomotion," *Robotics*, vol. 12, no. 1, 16, 2023.

[3] A. M. Abdullahi and R. Chaichaowarat, "Sensorless estimation of human joint torque for robust tracking control of lower-limb exoskeleton assistive gait rehabilitation," *J. Sens. Actuator Netw.*, vol. 12, no. 4, 53, 2023.

[4] R. Chaichaowarat, S. Nishimura, and H. I. Krebs, "Macro-mini linear actuator using electrorheological-fluid brake for impedance modulation in physical human–robot interaction," *IEEE Robot. Autom. Lett.*, vol. 7, no. 2, pp. 2945–2952, 2022.

[5] S. Nishimura, R. Chaichaowarat, and H. I. Krebs, "Human-robot interaction: controller design and stability," in *Proc. IEEE RAS/EMBS Int. Conf. Biomedical Robotics and Biomechatronics*, pp. 1096–1101, 2020.

[6] T. Tantagunninat, N. Wongkaewcharoen, K. Pornpipatsakul, R. Chuengpichanwanich, and R. Chaichaowarat, "Modulation of joint stiffness for controlling the cartesian stiffness of a 2-DOF planar robotic arm for rehabilitation," in *Proc. IEEE/ASME Int. Conf. Advanced Intelligent Mechatronics*, pp. 598–603, 2023.

[7] A. Javadi and R. Chaichaowarat, "Position and stiffness control of an antagonistic variable stiffness actuator with input delay using super-twisting sliding mode control," *Nonlinear Dyn.*, vol. 111, pp. 5359–5381, 2023.

[8] R. Chaichaowarat, S. Nishimura, and H. I. Krebs, "Design and modeling of a variable-stiffness spring mechanism for impedance modulation in physical human–robot interaction," in *Proc. IEEE Int. Conf. Robotics and Automation*, pp. 7052–7057, 2021.

[9] Z. Ullah, R. Chaichaowarat, and W. Wannasuphoprasit, "Variable damping actuator using an electromagnetic brake for impedance modulation in physical human–robot interaction," *Robotics*, vol. 12, no. 3, 80, 2023.

[10] R. Chaichaowarat, J. Kinugawa, and K. Kosuge, "Cycling enhance knee exoskeleton using planar spiral spring," in *Proc. IEEE/EMBS Annu. Int. Conf.*, pp. 3206–3211, 2018.

[11] R. Chaichaowarat, J. Kinugawa, A. Seino, and K. Kosuge, "A spring-embedded planetary-geared parallel elastic actuator," in *Proc. IEEE/ASME Int. Conf. Advanced Intelligent Mechatronics*, pp. 952–959, 2020.

[12] Y. Kim and Y. Cha, "Soft pneumatic gripper with a tendon-driven soft origami pump," *Front. Bioeng. Biotechnol.*, vol. 6, no. 461, pp. 1–11, 2020.

[13] D. Gonzalez, J. Garcia, R.M. Voyles, R.A. Nawrocki, and B. Newell, "Characterization of 3D printed pneumatic soft actuator," *Sens. Actuator A Phys.*, vol. 334, 113337, 2022.

[14] B.A.W. Keong and R.Y.C. Hua, "A novel fold-based design approach toward printable soft robotics using flexible 3D printing materials," *Adv. Mater. Technol.*, vol. 3, no. 2, 1700172, 2018.

[15] D. Herrero-Perez and H. Martinez-Berbera, "Soft gripper design and fabrication for underwater grasping," *Appl. Sci.*, vol. 12, 10694, 2022.

[16] A. Georgopoulou, B. Vanderborght, and F. Clemerns, "Fabrication of a soft robotic gripper with integrated strain sensing elements using multi-material additive manufacturing," *Front. Robot. AI.*, vol. 8, 615991, 2021.

[17] M. E. M. Salem, Q. Wang, R. Wen, and M. Xiang, "Design and characterization of soft pneumatic actuator for universal robot gripper," in *Proc. Int. Conf. Control and Robots*, pp. 6–10, 2018.

[18] C. Tawk, Y. Gao, R. Mutlu, and G. Alici, "Fully 3D printed monolithic soft gripper with high conformal grasping capability," in *Proc. IEEE/ASME Int. Conf. Advanced Intelligent Mechatronics*, pp. 1139–1144, 2019.

[19] R. Chaichaowarat, A. Sirichatchaikul, W. Iamkaew, and N. Phondee, "Affordable pipetting robot: gripper design for automatic changing of micropipette and liquid volume control," in *Proc. IEEE/ASME Int. Conf. Advanced Intelligent Mechatronics*, pp. 1275–1280, 2022.

[20] N. Phornpimonchoke, S. Koosermmit, A. Tanakijchumroon, and R. Chaichaowarat, "Alternative locomotion modalities for lunar rover," in *Proc. IEEE/ASME Int. Conf. Advanced Intelligent Mechatronics*, pp. 287–292, 2023.